Research Square

Preprints are preliminary reports that have not undergone peer review.
They should not be considered conclusive, used to inform clinical practice,
or referenced by the media as validated information.

Physics-Guided Ensemble Machine Learning for Predicting Concrete Carbonation Depth

Syeda Tabassum
Khulna University of Engineering and Technology
Badhon Singha
badhon10776@gmail.com
Ahsanullah University of Science and Technology
Sourov Karmakar
Ahsanullah University of Science and Technology

Research Article

Keywords: Concrete Carbonation Prediction, Physics-Guided Machine Learning, Explainable AI, XGBoost, SHAP Analysis

Posted Date: June 17th, 2026

DOI: https://doi.org/10.21203/rs.3.rs-9961154/v1

License: This work is licensed under a Creative Commons Attribution 4.0 International License.
Read Full License

Additional Declarations: No competing interests reported.

Physics-Guided Ensemble Machine Learning for Predicting Concrete Carbonation Depth

Syeda Tabassum [1], Badhon Singha [2] orcid and Sourav Karmakar [3]

[1] Department of Building Engineering and Construction Management, Khulna University of Engineering and Technology, Khulna, Bangladesh

[2,3] Department of Civil Engineering, Ahsanullah University of Science and Technology, Dhaka, Bangladesh

Corresponding Author: Badhon Singha

Corresponding Author's Email: badhon10776@gmail.com

Abstract

Accurate prediction of concrete carbonation is critical for durability design and service life evaluation, but traditional carbonation models frequently fail to represent the complex nonlinear interplay between material qualities, ambient variables, and exposure history. This paper provides a physics-guided machine learning system that uses the classical square-root-of-time carbonation rule to predict the carbonation coefficient rather than the carbonation depth directly. A comprehensive database of 2,147 samples collected from 46 experimental studies was assembled, covering diverse mix compositions, curing regimes, and exposure environments. Four machine learning algorithms Random Forest, XGBoost, LightGBM, and Artificial Neural Network were developed using physics-informed interaction features, including w/b × CO_2 and RH × T. Among the investigated models, XGBoost achieved the best performance, yielding R^2 = 0.8884, RMSE = 0.6766 mm/√d, and MAE = 0.4020 mm/√d for carbonation coefficient prediction, and R^2 = 0.8965, RMSE = 4.18 mm, and MAE = 2.54 mm for reconstructed carbonation depth. Compared with the fib Model Code 2010 and DuraCrete models, XGBoost reduced RMSE by approximately 77% and MAE by more than 80%, demonstrating substantially improved predictive accuracy. Ten-fold cross-validation confirmed robust predictive performance within the domain represented by the compiled database (mean R^2 = 0.8807 ± 0.0164). SHAP and permutation importance analyses identified the w/b × CO_2 interaction, carbonation time, RH × T interaction, cement content, and water-to-binder ratio as the dominant predictors. The proposed framework provides an accurate, interpretable, and physically consistent tool for carbonation prediction, supporting durability-based design and service-life management of reinforced concrete structures.

Keywords*: Concrete Carbonation Prediction; Physics-Guided Machine Learning; Explainable AI; XGBoost; SHAP Analysis.*

1 Introduction

Carbonation-induced corrosion is one of the leading causes of long-term deterioration in reinforced concrete (RC) worldwide, with corrosion-related damage to materials and sectors estimated to cost several trillion in annual global costs [1]. Carbonation lowers the pH of the concrete pore solution, eventually destroying the passive layer on steel, allowing for active corrosion in the presence of moisture and oxygen [2–5]. The deterioration initiates with the diffusion of CO_2 through the concrete pore network, its dissolution in the pore solution, and subsequent reaction with calcium hydroxide

(portlandite) to form calcium carbonate [6,7]. The chemical reaction responsible for this process can be expressed as:

$$Ca(OH)_2 + CO_2 \rightarrow CaCO_3 + H_2O \quad (1)$$

This carbonation reaction consumes the alkaline species that maintain a high pH (≈12.5-13) in the pore solution, progressively lowering it to values near or below 9 [8,9]. Once the pH falls below the threshold for passivity, the protective oxide film on the reinforcing steel destabilizes (depassivation), and in the presence of moisture and oxygen, electrochemical corrosion initiates. The resulting expansive rust products generate tensile stresses that crack and spall the concrete cover, ultimately reducing the cross-sectional area of the steel and impairing structural capacity [9–11]. Accurate prediction of carbonation depth is fundamental to durability-based design, service-life estimation, and maintenance planning for reinforced concrete (RC) structures. Service-life prediction frameworks routinely embed carbonation models to estimate the time to depassivation of embedded steel reinforcement, thereby guiding critical decisions regarding concrete mixture design, cover thickness, admixture selection and the selection of appropriate protective measures [12].

Among the various approaches developed to predict carbonation progression in concrete, the diffusion-based relationship remains the most widely employed in both research and engineering practice:

$$x_c = k_c\sqrt{t} \quad (2)$$

In this expression, x_c denotes the carbonation depth (mm), k_c is the carbonation coefficient, and t is the elapsed exposure time (years). Derived from Fick's law of diffusion, this model is widely adopted owing to its mathematical simplicity and empirical validation across diverse concrete types and exposure environments [13,14]. By incorporating such predictions into the design process, engineers can assess the long-term durability of RC structures and make informed decisions regarding mixture composition, cover thickness, and protective measures to delay steel depassivation beyond the target service life [10,15]. At a broader level, integration of these models into service-life design frameworks supports the development of infrastructure that is structurally reliable, economically viable, and environmentally sustainable, while also guiding maintenance planning for existing assets.

Conventional approaches to carbonation prediction rely on semi-empirical formulations that combine simplified transport theory with parameters calibrated from limited experimental datasets. These models typically use Fick's Second Law of Diffusion to establish a standard square-root-of-time relationship, where the depth of carbonation grows proportionally to the square root of exposure time[16]. The necessary scaling factors are then determined by fitting these mathematical curves to empirical data gathered from short-term laboratory experiments or localized field exposures. While this hybrid approach offers mathematical simplicity and low computational costs, it introduces severe limitations in long-term durability forecasting. Models calibrated on short-term data or accelerated testing environments often fail to extrapolate accurately over 50- to 100-year structural lifespans. Furthermore, these simplified formulations cannot dynamically adapt to fluctuating environmental microclimates, such as cycling relative humidity and temperature, nor can they accurately predict the behavior of

modern, low-carbon binders like fly ash, slag, or calcined clays without extensive and costly recalibration. However, their predictive capability is fundamentally constrained when applied to modern concrete systems. Real carbonation behavior is not governed by a single linear relationship, but by highly coupled interactions among material composition, curing history, pore structure, humidity, temperature, CO2 concentration, cracking, and aging effects. Since traditional models reduce this complexity to a small number of parameters, they often struggle to represent nonlinear behavior and to generalize across different mixtures and exposure scenarios.

This limitation becomes more pronounced in concretes containing supplementary cementitious materials (SCMs) such as fly ash, slag, or silica fume. SCMs can alter hydration kinetics, refine or modify pore structure, change the availability of portlandite, and affect buffering capacity, all of which influence carbonation resistance in ways that are not fully captured by classical models. In addition, SCM-based mixtures often require different curing regimes, and insufficient curing can further amplify carbonation susceptibility, creating behavior that is difficult to predict using conventional equations alone.

The rapid growth of machine learning (ML) in structural and materials engineering has opened new pathways for addressing the limitations of classical carbonation models. ML-based approaches, particularly ensemble tree methods and neural networks, can learn complex, nonlinear input-output relationships directly from experimental data without requiring explicit analytical formulations. Recent studies have demonstrated that models such as random forests, gradient boosting, and artificial neural networks can achieve significantly higher predictive accuracy than traditional empirical equations for concrete carbonation depth prediction.

However, most existing ML-based carbonation models suffer from two key shortcomings. First, they predict carbonation depth X directly, without embedding the governing physical law into the model structure. This exposes predictions to inconsistency with the established square-root-of-time mechanism particularly when models are applied outside their training data range or to different exposure durations. Second, existing studies often rely on small, single-source datasets with limited variability in mix design and environmental conditions, restricting their generalizability. Furthermore, few studies systematically validate feature importance through rigorous explainability methods or compare physics-guided ML outputs against classical models on a common multi-source benchmark.

This limitation becomes more pronounced in concretes containing supplementary cementitious materials (SCMs) such as fly ash, slag, or silica fume. SCMs can alter hydration kinetics, refine or modify pore structure, change the availability of portlandite, and affect buffering capacity, all of which influence carbonation resistance in ways that are not fully captured by classical models [17]. In addition, SCM-based mixtures often require different curing regimes, and insufficient curing can further amplify carbonation susceptibility, creating behavior that is difficult to predict using conventional equations alone. To address these limitations, the specific objectives of this study are:

1. To develop and optimize physics-guided Random Forest, XGBoost, LightGBM, and ANN models for predicting carbonation coefficient and depth of concrete using a large multi-source experimental database, and to demonstrate reliable performance within the range of mix designs and exposure conditions represented in the dataset.
2. To evaluate and validate the predictive capability and robustness of the developed models through statistical performance metrics, cross-validation, uncertainty analysis, and comparison with established classical carbonation models.
3. To interpret the developed ML framework using explainable AI techniques (SHAP and permutation importance) in order to identify the dominant factors governing carbonation depth and support durability-based structural design and service-life assessment.

2 Research Framework

This study proposes a physics-guided machine learning (PGML) framework for predicting concrete carbonation, integrating domain knowledge with data-driven modeling to ensure both physical consistency and predictive accuracy. Unlike conventional approaches that directly estimate carbonation depth (X), the present framework predicts the carbonation coefficient (k), which is subsequently used to reconstruct depth through the well-established square-root-of-time relationship. This strategy embeds physical laws into the learning process and reduces model inconsistency. The overall workflow is structured into four sequential stages illustrated in Figure 1:

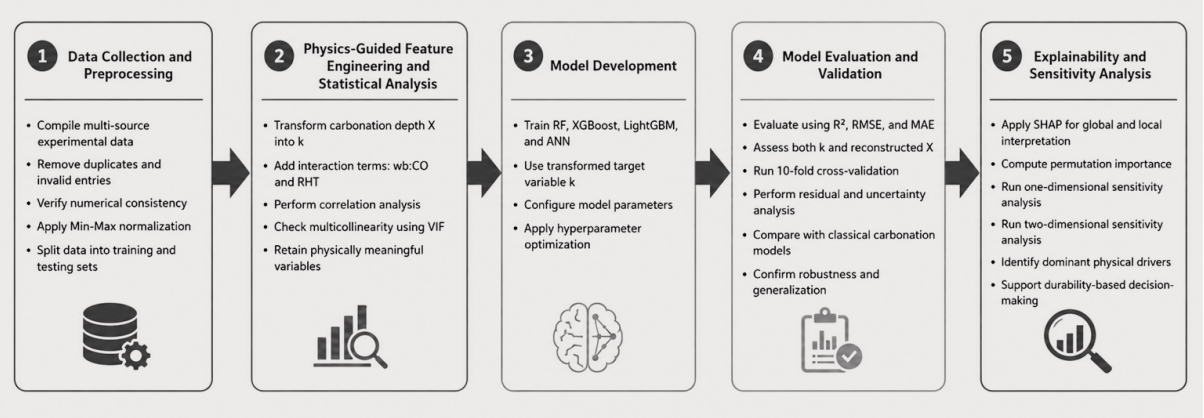


Figure 1: Physics-guided machine learning workflow for concrete carbonation prediction.

2.1 Data Collection and Preprocessing

A dataset of 2,147 samples was compiled from 46 experimental studies, including mix design, environmental, and time-related variables.

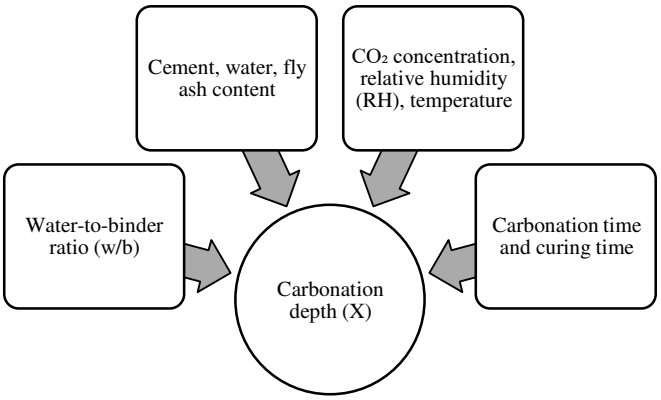


Figure 2: Key parameters influencing concrete carbonation depth

Data preprocessing included:

Removal of duplicates (15 rows)

Verification of numerical consistency

Elimination of invalid entries (e.g., zero carbonation time)

Descriptive statistical analysis was conducted to understand data distribution, revealing skewness in carbonation depth and variability in exposure conditions.

2.2 Physics-Guided Feature Engineering and Statistical Analysis

2.2.1 Target Transformation

The study adopts a physics-oriented strategy to improve the robustness and interpretation of machine learning models. According to established carbonation theory, carbonation depth follows a square-root-of-time relationship:

$$X = k\sqrt{t} \tag{4}$$

where X denotes carbonation depth, t is exposure time, and k represents the carbonation coefficient, which characterizes the resistance of concrete against CO_2 ingress.

Rather than directly predicting carbonation depth (X), the target variable is transformed into the carbonation coefficient (k) using:

$$k = \frac{X}{\sqrt{t}} \tag{5}$$

This transformation embeds the governing physical mechanism into the data-driven framework. By expressing carbonation behavior in terms of the carbonation coefficient (k), the dominant square-root-of-time scaling effect inherent in carbonation depth measurements is reduced, allowing the model to focus more directly on material and environmental influences. However, carbonation time was retained as an input feature because practical carbonation behavior is affected by additional time-dependent mechanisms, including continued hydration, microstructural evolution, moisture redistribution, and exposure-history effects. Consequently, the transformed coefficient should be interpreted as an effective

carbonation coefficient derived from experimental observations rather than a strictly time-independent material constant. This approach preserves consistency with the established carbonation law while enabling the model to capture residual temporal effects present in real-world experimental datasets.

After model training, the carbonation depth is reconstructed using the predicted carbonation coefficient:

$$X_{\text{pred}} = k_{\text{pred}} \cdot \sqrt{t} \tag{6}$$

This ensures that the final predicted values strictly conform to the theoretical carbonation law while leveraging the predictive capability of machine learning.

2.2.2 Interaction Features and Correlation Analysis

Additional interaction characteristics have been introduced to better capture the nonlinear interaction between material properties and environmental conditions. Specifically, two terms of physical meaning interaction were considered:

$$\left(\frac{w}{b}\right) \times CO_2 \tag{7}$$

$$RH \times T \tag{8}$$

The first interaction term reflects the combined influence of pore structure (governed by water-to-binder ratio) and CO_2 concentration on carbonation rate. The second term represents the coupled effect of relative humidity and temperature, both of which significantly influence CO_2 diffusion and chemical reaction kinetics.

Correlation analysis was conducted to evaluate the relationship between input variables and the transformed target variable (k). The results indicate that exposure time–related variables and environmental factors (e.g., relative humidity, temperature, and CO_2 concentration) exert a dominant influence on carbonation behavior. In contrast, mix design parameters such as water-to-binder ratio and binder content exhibit comparatively secondary effects, although they remain important for long-term durability.

To assess multicollinearity among the features, the Variance Inflation Factor (VIF) was computed. Some interaction terms exhibited relatively high VIF values because of their inherent correlation with the parent variables. Nevertheless, these features were retained in the model due to their strong physical relevance. Additionally, certain machine learning algorithms particularly tree-based ensemble methods are inherently robust to multicollinearity and can effectively handle correlated predictors without substantial loss of performance. The combined use of physics-informed interaction features and statistical evaluation enhances the model's capacity to represent complex carbon dioxide dynamics while preserving both interpretability and predictive accuracy.

2.3 Model Development

2.3.1 Data Preparation

The dataset was first divided into training and testing subsets using an 80:20 ratio with a fixed random state of 42 to ensure reproducibility. Min–Max normalization was then fitted exclusively on the training

dataset, and the resulting scaling parameters were subsequently applied to transform both the training and testing datasets. This procedure prevents information leakage from the testing set into the training process and ensures an unbiased evaluation of model performance. All input features were scaled to the range [0,1]. A summary of the data preprocessing is presented in Table 1.

In accordance with the physics-guided framework, the target variable was transformed from carbonation depth (X) to carbonation coefficient (k) prior to training.

Table 1: Data Preparation Summary

Step	Description
Data normalization	Min-Max scaling applied to all features
Feature range	Scaled to [0, 1]
Data split	80% training, 20% testing
Random state	42 (for reproducibility)
Target variable	Transformed from X to k

2.3.2 Machine Learning Models

To capture the complex nonlinear relationships, present in the assembled dataset, four machine learning models were developed: Random Forest (RF), XGBoost, LightGBM, and Artificial Neural Network (ANN). These models were selected due to their proven effectiveness in handling tabular engineering data and nonlinear feature interaction. Tree-based ensemble models were prioritized due to their robustness to multicollinearity and ability to handle tabular engineering data without extensive preprocessing.

The ensemble models (RF, XGBoost, and LightGBM) were configured with 300 estimators to ensure sufficient model capacity. For boosting-based models, a learning rate of 0.05 was used to achieve stable and gradual learning. The detailed configuration of each model is summarized in Table 2.

The ANN model was designed as a multilayer feedforward network with three hidden layers consisting of 128, 64, and 32 neurons. The Rectified Linear Unit (ReLU) activation function was used to introduce nonlinearity, and the Adam optimizer was adopted for efficient training.

Table 2: Machine Learning Model Configuration

Model	**Type**	**Key Parameters**
Random Forest (RF)	Bagging ensemble	n_estimators = 300
XGBoost	Boosting ensemble	n_estimators = 300, learning_rate = 0.05

LightGBM	Boosting ensemble	n_estimators = 300, learning_rate = 0.05
ANN	Deep learning	Layers = (128, 64, 32), Activation = ReLU, Optimizer = Adam

All models were trained using the transformed carbonation coefficient (k), ensuring consistency with the underlying physical formulation. This approach enables the models to learn intrinsic material and environmental effects while maintaining alignment with carbonation theory.

2.4 Model Evaluation and Validation

The performance of the developed models was evaluated using multiple statistical metrics to ensure predictive accuracy and robustness. Specifically, the coefficient of determination (R^2), root mean square error (RMSE), and mean absolute error (MAE) were employed to assess model performance from complementary perspectives, including goodness-of-fit and the magnitude of prediction errors.

To maintain consistency with the physics-guided framework, model evaluation was conducted at two levels: (i) prediction of the carbonation coefficient (k) and (ii) reconstruction of carbonation depth (X) using the inverse transformation. This dual-level assessment ensures that the models are both mathematically accurate and practically applicable for engineering predictions of carbonation depth.

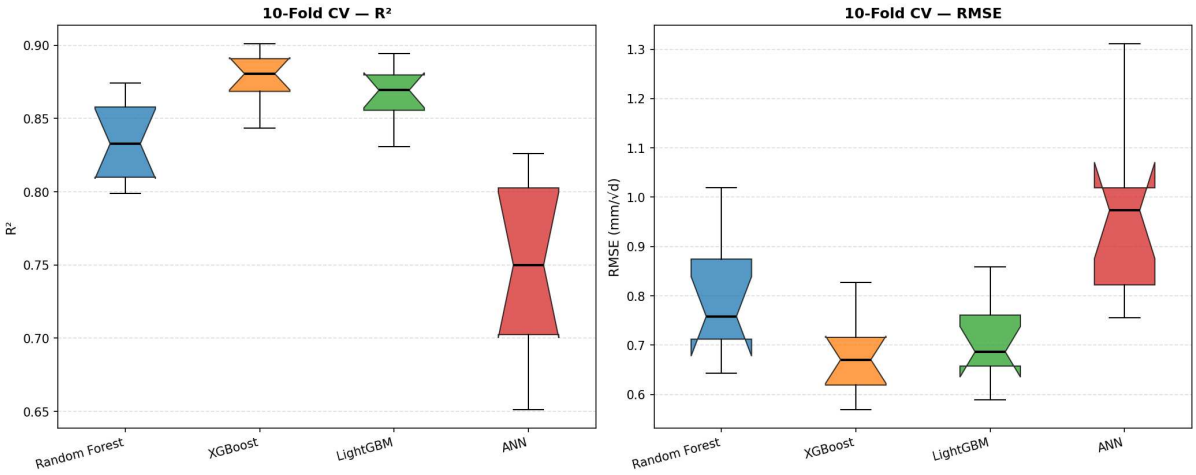


Figure 3: 10-fold cross-validation results (R^2 and RMSE) of the four machine-learning models

To further improve model reliability. a 10-fold cross-validation approach was implemented. In this procedure, the dataset was randomly divided into ten subsets, and model training and validation were performed iteratively to reduce the influence of data partitioning bias. In addition, Bayesian hyperparameter optimization using the Tree-structured Parzen Estimator (TPE) was applied to XGBoost and LightGBM over 50 trials to identify optimal configurations. Residual analysis was also carried out to examine the distribution of prediction errors and to identify any systematic bias or heteroscedasticity. These validation strategies collectively confirm the generalization capability and stability of the developed models across diverse data conditions.

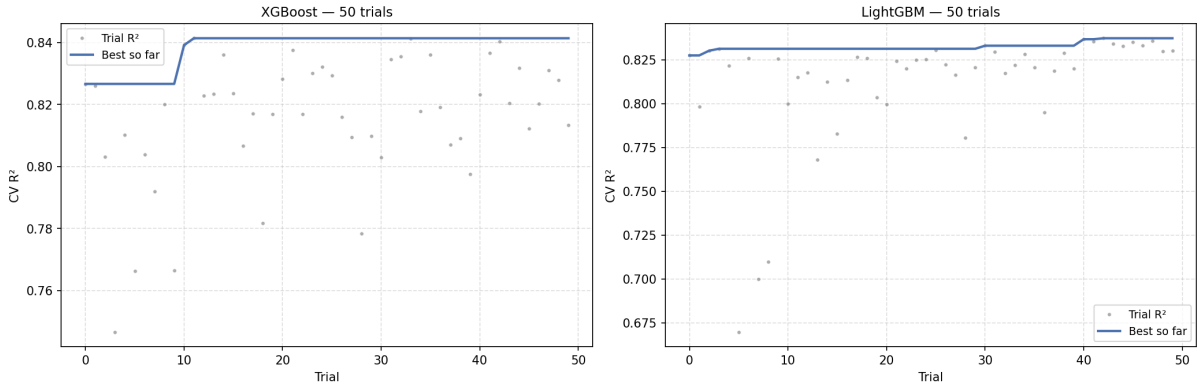


Figure 4: Bayesian optimization convergence of XGBoost and LightGBM over 50 Optuna-TPE trials (CV R^2)

2.5 Explainability and Sensitivity Analysis

To enhance model transparency and facilitate engineering interpretation, both explainability and sensitivity analyses were conducted based on the trained models and underlying dataset.

2.5.1 SHAP Analysis

SHAP (SHapley Additive Explanations) was employed to interpret model predictions by quantifying the contribution of each input feature to the predicted carbonation coefficient (k). This method provides a unified framework for both global and local interpretability.

At the global level, SHAP analysis identifies the most influential variables governing carbonation behavior across the entire dataset, enabling ranking of feature importance. At the local level, it explains individual predictions by illustrating how each feature contributes either positively or negatively to the predicted outcome.

Moreover, SHAP analysis facilitates the identification of nonlinear relationships and interaction effects among variables, providing deeper insight into the coupled influence of material properties and environmental conditions on carbonation.

2.5.2 Sensitivity Analysis

Sensitivity analysis was conducted to systematically evaluate the influence of key input parameters on carbonation behavior. A one-dimensional sensitivity analysis was first performed, where individual parameters were varied independently while keeping other variables constant. This approach allows clear assessment of the isolated effect of each parameter.

In addition, a two-dimensional sensitivity analysis was carried out by simultaneously varying critical variables such as water-to-binder ratio and CO_2 concentration to capture interaction effects. This approach provides a more realistic representation of field conditions, where multiple factors influence carbonation simultaneously.

3 Results and Analysis

3.1 Dataset Overview and Key Statistics

The final dataset comprises N = 2,147 cleaned samples with 11 input variables, representing mix design parameters, environmental conditions, and exposure duration.

As presented in Table 3, the dataset spans a wide range of carbonation-influencing conditions. The water-to-binder ratio (w/b) varies from 0.26 to 0.77, while CO_2 concentration ranges from 0.03% to 100%, indicating inclusion of both natural and accelerated carbonation environments. Environmental variables such as relative humidity (40-90%) and temperature (6°-45°C) show comparatively narrower ranges, reflecting controlled experimental conditions. The carbonation exposure time (√t) extends from 1.73 to 68.72 √days, covering both short- and long-term behavior.

In terms of variability, CO_2 concentration, fly ash content, and cement content exhibit high dispersion, whereas relative humidity shows relatively low variability, indicating stable environmental control across studies. Furthermore, the dataset demonstrates non-uniform distributions, with skewness observed in CO_2 and carbonation-related variables, while the w/b ratio remains approximately normally distributed.

Table 3: Descriptive Statistics of the Variables

Variable	**Unit**	**Min**	**Max**	**Mean**	**Std. Dev**
Cement	kg/m³	67.00	513.00	267.21	91.55
Water	kg/m³	97.00	280.30	169.85	23.87
Fly Ash (SCM)	kg/m³	0.00	373.00	54.31	86.99
w/b ratio	-	0.26	0.77	0.492	0.088
CO_2 concentration	%	0.03	100.00	12.74	15.01
(w/b × CO_2)	%²	0.01	55.00	6.14	7.19
Relative Humidity (RH)	%	40.00	90.00	67.71	5.50
Temperature	°C	6.00	45.00	20.72	5.79
(RH × T)	%·°C	420.00	2970.00	1387.75	352.62
Carbonation time (√t)	√days	1.73	68.72	12.01	13.76
Curing time	days	1.00	1123.00	53.81	150.16

3.2 Target Variable Behavior and Physical Consistency

The behavior of carbonation depth (x) was evaluated using the experimental dataset (N = 2,147). As shown in Figure 5, the distribution of carbonation depth (x) is strongly right-skewed, with most values

concentrated below approximately 20-25 mm, while a long tail extends beyond 60 mm. This indicates high variability and non-uniformity in carbonation depth, suggesting that carbonation depth (x) is influenced by multiple interacting factors and is not statistically stable as a direct prediction target.

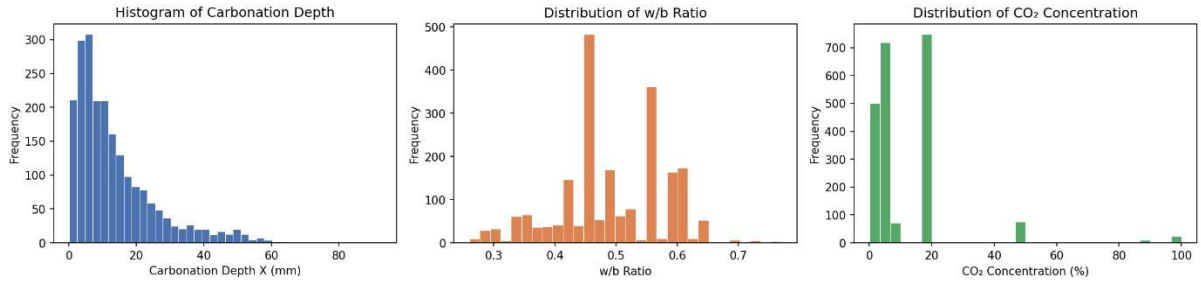


Figure 5: Distributions of carbonation depth, water-to-binder ratio, and CO_2 concentration.

In contrast, the carbonation coefficient (k), derived from the same dataset, exhibits a comparatively more compact and symmetric distribution, as illustrated in Figure 6 . The values of k range from 0.017 to 18.11 mm/√d, but most observations are concentrated within a narrower band (approximately 0-5 mm/√d). This reduced spread demonstrates that transforming x into k effectively minimizes dispersion caused by exposure conditions, particularly time.

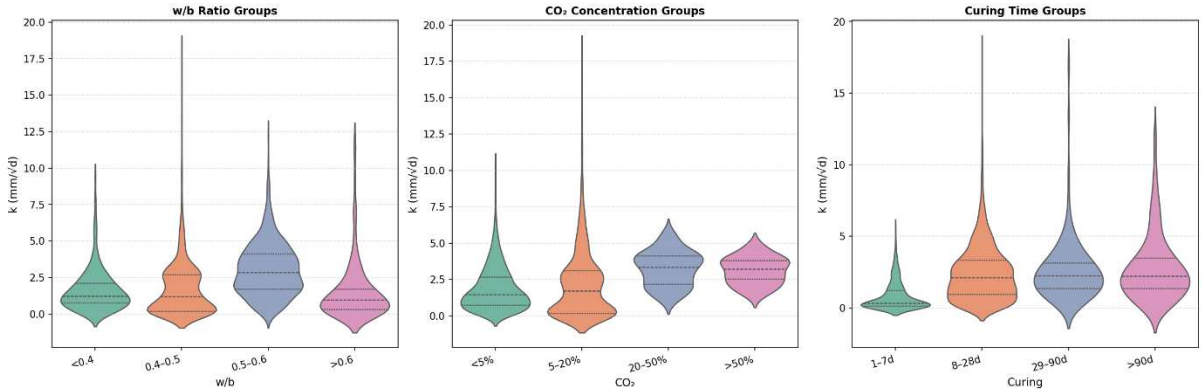


Figure 6: Carbonation coefficient k distributions by parameter groups.

Further insight is obtained from the correlation heatmap Figure 7, which shows the relationships between input variables and k. The heatmap indicates clear and physically meaningful correlations, particularly for interaction terms such as (w/b × CO_2) and (RH × T), as well as carbonation time (√t). Compared to depth-based variability, these relationships appear more structured and less noisy, confirming improved consistency in the transformed target.

Overall, the dataset-driven analysis confirms that carbonation depth (x) is highly skewed and statistically unstable, whereas the carbonation coefficient (k) provides a more uniform and physically interpretable representation, making it a more suitable target for machine learning modelling.

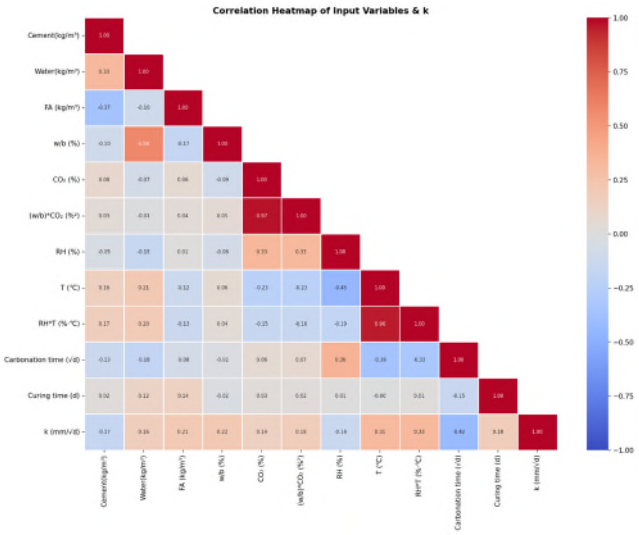


Figure 7: Pearson correlation heatmap

3.3 Model Performance Evaluation

The predictive performance of all machine learning models was evaluated using the test dataset, with results summarized in Tables 4 and 5. The evaluation metrics include the coefficient of determination (R^2), root mean square error (RMSE), and mean absolute error (MAE), representing goodness-of-fit and prediction accuracy.

3.3.1 Prediction of Carbonation Coefficient (k)

Table 4: Model Performance for Carbonation Coefficient (k)

Model	R^2	RMSE (mm/√d)	MAE (mm/√d)	Rank
XGBoost	0.8884	0.6766	0.4020	1st
LightGBM	0.8659	0.7416	0.4004	2nd
Random Forest	0.8140	0.8735	0.5011	3rd
ANN (MLP)	0.7763	0.9579	0.6076	4th

The results indicate that XGBoost achieves the highest prediction accuracy with an R^2 of 0.8884, RMSE of 0.6766 mm/√d, and MAE of 0.4020 mm/√d. This demonstrates its strong capability in capturing the nonlinear relationships governing carbonation behavior.

LightGBM shows comparable performance with slightly lower R^2 (0.8659) and higher RMSE, while Random Forest exhibits moderate accuracy. In contrast, the ANN model produces the lowest performance with higher prediction errors. Overall, tree-based ensemble models consistently outperform the neural network approach.

Table 5: Model Performance for Carbonation Depth (X)

Model	R^2	RMSE (mm)	MAE (mm)	Rank
XGBoost	0.8965	4.18	2.54	1st
LightGBM	0.8936	4.24	2.41	2nd
Random Forest	0.8732	4.63	2.94	3rd
ANN (MLP)	0.7989	5.83	4.02	4th

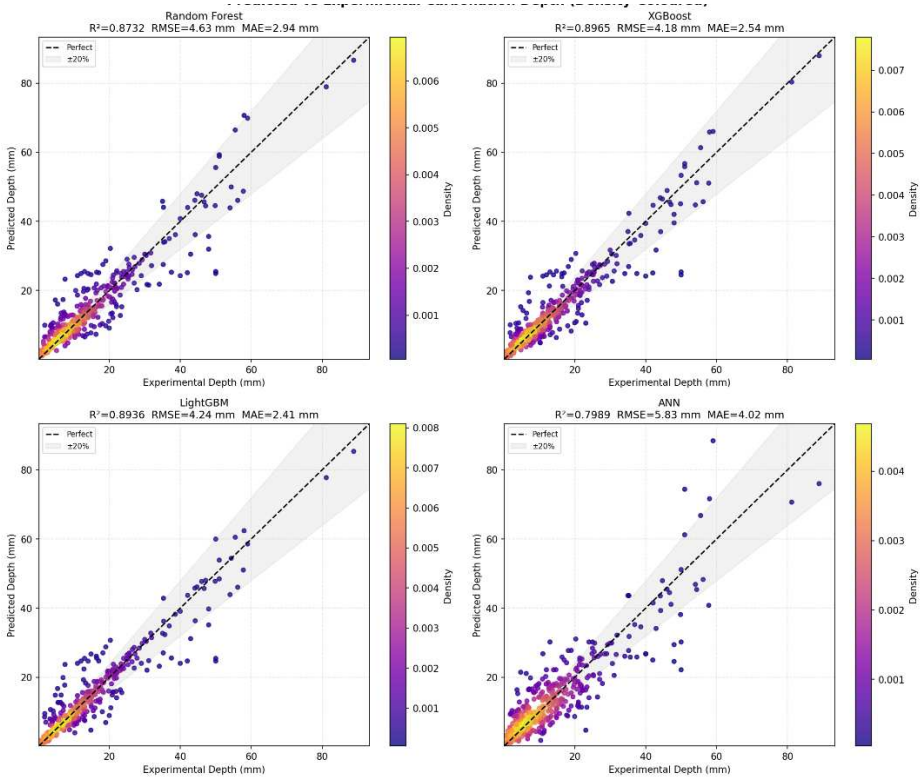


Figure 8: Predicted versus experimental carbonation depth for the four machine-learning models (density-colored parity plots).

XGBoost again achieved the best overall performance with an R^2 of 0.8965, indicating excellent agreement between predicted and experimental carbonation depth. The RMSE of 4.18 mm and MAE of 2.54 mm confirm high prediction accuracy within practical engineering limits.

Although LightGBM shows slightly lower MAE (2.41 mm), its overall performance is marginally inferior due to slightly lower R^2 and higher RMSE. Random Forest and ANN follow similar performance trends as observed in k prediction.

3.3.2 Ablation Analysis of the Physics-Guided Framework

To quantify the contribution of the physics-guided components, an ablation study was conducted given in Table 6. Three XGBoost configurations were evaluated: a baseline model predicting carbonation depth directly, a model predicting the carbonation coefficient without interaction features, and the

proposed physics-guided model incorporating both the carbonation coefficient transformation and physically meaningful interaction terms. The proposed framework achieved the best overall performance, with R^2 = 0.8989, RMSE = 4.21 mm, and MAE = 2.58 mm. Although the numerical improvement over the baseline model was modest, the physics-guided formulation improved physical interpretability while maintaining consistency with established carbonation theory.

Table 6: Ablation analysis of the proposed physics-guided machine learning framework for carbonation prediction.

Model	**Target**	**Physics Features**	**R^2**	**RMSE**	**MAE**
Baseline	Depth	None	0.8982	4.219	2.628
k-based	k	None	0.8937	4.311	2.645
PGML	k	wb×CO_2 + RH×T	0.8989	4.206	2.578

3.4 Feature importance and physical interpretation

Global explainability of the physics-guided ML models was analyzed using SHAP on the best-performing XGBoost model, along with permutation importance and feature importance comparisons among the three tree-based models. The combined analysis identifies the key factors influencing the carbonation coefficient k and links the statistical results with the underlying carbonation behavior.

Across all methods, the interaction term $w/b \times CO_2$was identified as the most influential predictor, followed by carbonation time, the thermo-hygric interaction index RHT, cement content, and the water-to-binder ratio w/b. SHAP analysis of the XGBoost model confirmed this ranking, with mean absolute SHAP values of 0.4627 for w/b*CO_2, 0.4277 for carbonation time, 0.3853 for RHT, 0.2911 for cement, and 0.1870 for w/b, while the remaining features showed much smaller effects. Figure 11 presents the normalized feature importance obtained from, XGBoost showing variables were consistently ranked as the most important. This consistency suggests that the identified importance pattern reflects stable relationships within the dataset rather than the behavior of a single model.

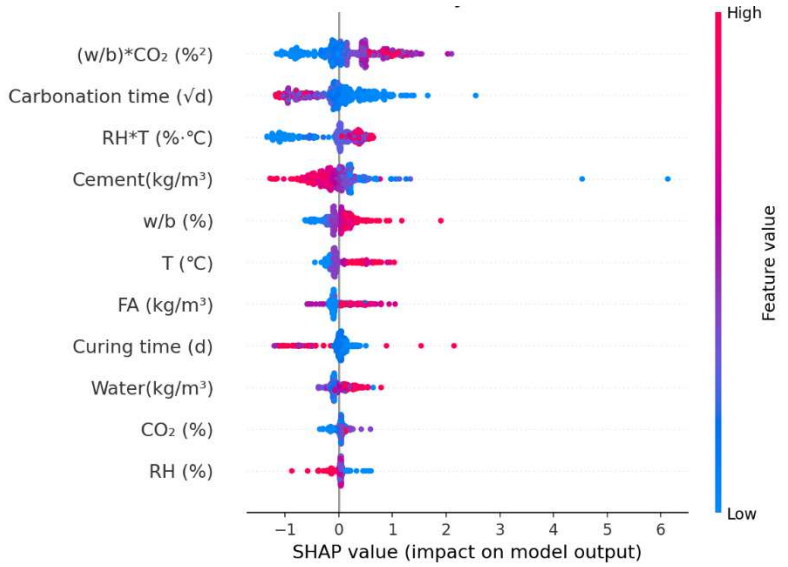


Figure 9: SHAP summary plot of feature importance for the XGBoost carbonation coefficient model.

The strong influence of $\frac{w}{b} * CO_2$ reflects the combined effect of concrete porosity and CO_2 exposure on carbonation. This interaction term combines the water-to-binder ratio, which controls pore structure and diffusivity, with CO_2 concentration, which controls environmental severity. Higher $\frac{w}{b} * CO_2$values therefore produce faster carbonation. SHAP plots showed that increasing $\frac{w}{b} * CO_2$ increases the carbonation coefficient k, consistent with diffusion-based carbonation theory and the sensitivity analysis of w/b-CO_2 interactions.

Carbonation time was the second most important parameter and represents exposure duration in the carbonation relationship $X = k\sqrt{t}$. Longer exposure periods amplify differences in diffusivity and buffering capacity between mixtures, allowing the model to better distinguish between slow and rapid carbonation behavior.

The thermo-hygric interaction index RHT was the third major contributor. It combines temperature and relative humidity and captures their coupled influence on carbonation. SHAP analysis showed that RHT was more influential than temperature or humidity alone and had strong nonlinear interactions with w/bCO_2. Intermediate moisture conditions favor carbonation, while very dry or saturated conditions reduce it.

Cement content ranked fourth because it influences both calcium hydroxide availability and pore refinement. Variations in cement dosage significantly affected predicted carbonation coefficients, reflecting its role in alkalinity and permeability development. The water-to-binder ratio w/b remained an important independent variable, despite being partly included in w/b*CO_2. Higher w/bvalues create coarser pore networks and higher diffusivity, leading to larger carbonation coefficients. Overall, SHAP and permutation analyses showed that carbonation behavior is mainly governed by the interaction between pore structure parameters (w/bCO_2, cement, and w/b) and environmental conditions (time, CO_2 concentration, and RHT).

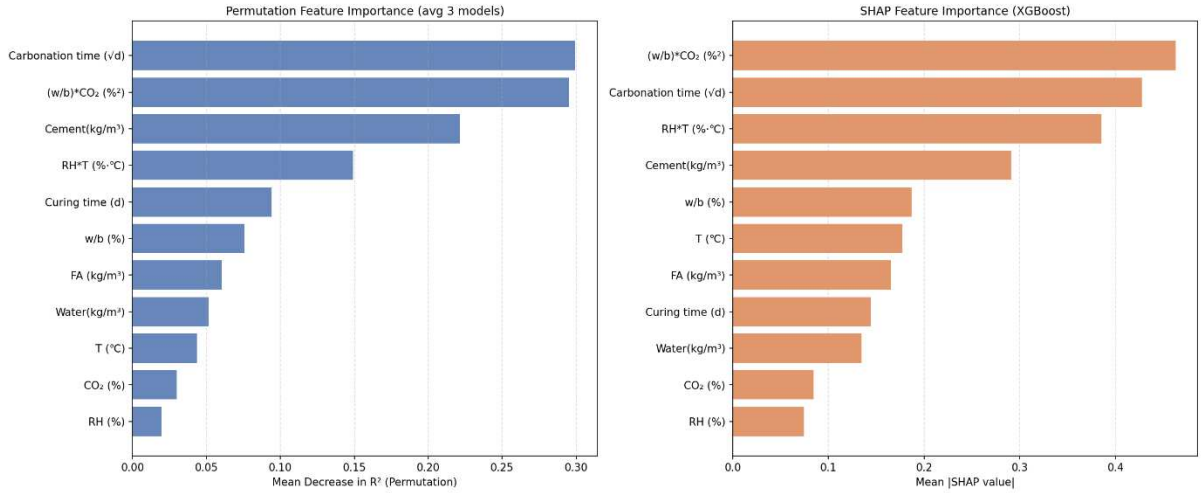


Figure 10: Comparison of permutation and SHAP feature importance rankings for carbonation coefficient prediction.

To verify the reliability of the results, permutation importance averaged across Random Forest, XGBoost, and LightGBM was compared with SHAP importance from the XGBoost model. Figure Y shows that both methods produced very similar feature rankings, with $w/b * CO_2$, carbonation time, RHT, and cement consistently appearing as the most influential variables, while the remaining features had much smaller contributions.

A small difference was observed between the two methods. Permutation importance ranked carbonation time slightly higher than $w/b * CO_2$, whereas SHAP identified $w/b * CO_2$ as the most important feature. This is reasonable because permutation importance measures how much the model performance decreases when a variable is randomly shuffled. Since the dataset contains a wide range of exposure durations, carbonation time strongly affects the overall model accuracy and R^2. In contrast, SHAP explains individual predictions and therefore gives more importance to $w/b * CO_2$, which represents the combined effect of pore structure and CO_2 exposure that directly controls carbonation behavior.

Overall, the close agreement between permutation importance and SHAP indicates that the identified key variables represent meaningful physical relationships rather than effects specific to a single explainability method.

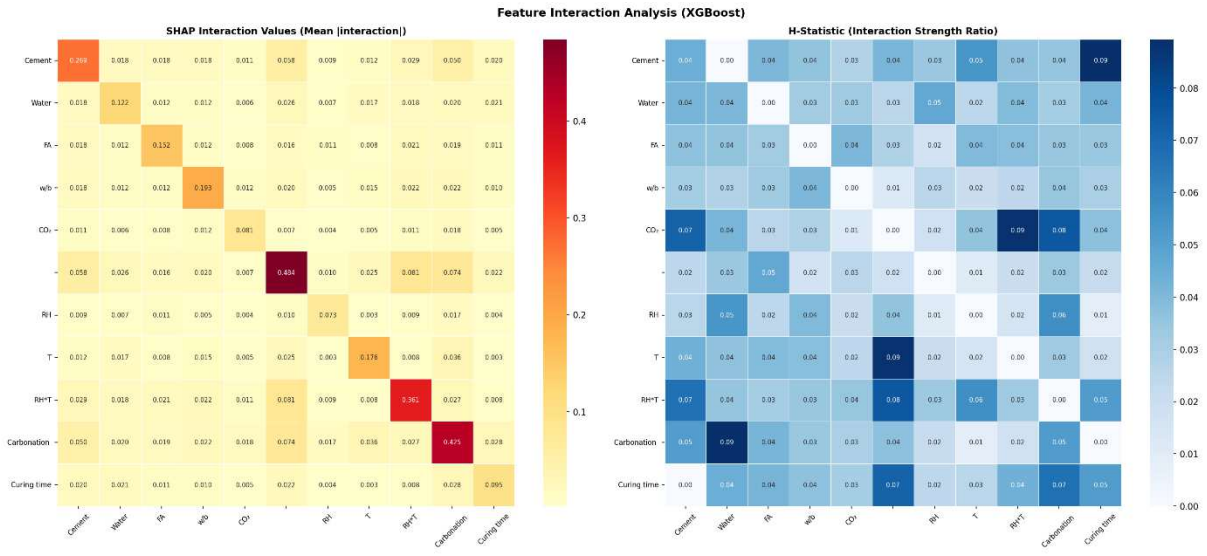


Figure 11: Feature interaction analysis using SHAP interaction values and H-statistic for the XGBoost model

SHAP interaction values and Friedman's H-statistic were computed shown in Figure 12. The (w/b) × CO_2 term showed the highest self-interaction magnitude (0.484), followed by RH×T (0.361) and carbonation time (0.425), confirming that the engineered interaction features capture dominant non-linear physical cross-dependencies rather than redundant information.

3.5 Sensitivity Analysis and Mix Design Implications

A two-dimensional sensitivity analysis was carried out to evaluate the combined influence of the water-to-binder ratio w/b and CO_2 concentration on predicted carbonation depth, while keeping all other variables at their median values. The contour plot shows low carbonation depths at low w/b and low CO_2 levels, followed by a rapid increase as both parameters rise. The corresponding 3D surface (Fig. Z, right) shows a relatively flat low-risk region at low w/b and CO_2, and a steep increase in carbonation depth toward the high-w/b, high-CO_2 region.

Within the investigated range ($w/b \approx 0.35 - 0.60$ and $CO_2 \approx 0$–50%), the contour lines clearly indicate a strong interaction between the two variables. At high CO_2 concentrations, even small increases in w/b produce a significant increase in carbonation depth, whereas the same change has a smaller effect under low CO_2 conditions. This behavior agrees well with the SHAP and permutation importance analyses, which identified both w/b and w/b*CO_2 as key drivers of the carbonation coefficient k.

The sensitivity analysis also provides several practical implications for mix design. Lower w/b values are particularly important in aggressive CO_2 environments, as they help maintain lower carbonation depths even under elevated exposure conditions. The one-dimensional sensitivity curves further show that extended curing can reduce carbonation depth, especially for mixtures with higher w/bvalues, suggesting that improved curing can partly compensate for less favorable mix proportions. In cases where low w/b cannot be achieved, limiting CO_2 exposure through adequate cover or surface protection becomes increasingly important.

For brevity, only the two-dimensional w/b*CO_2 contour plot and the corresponding 3D response surface are included in the main text.

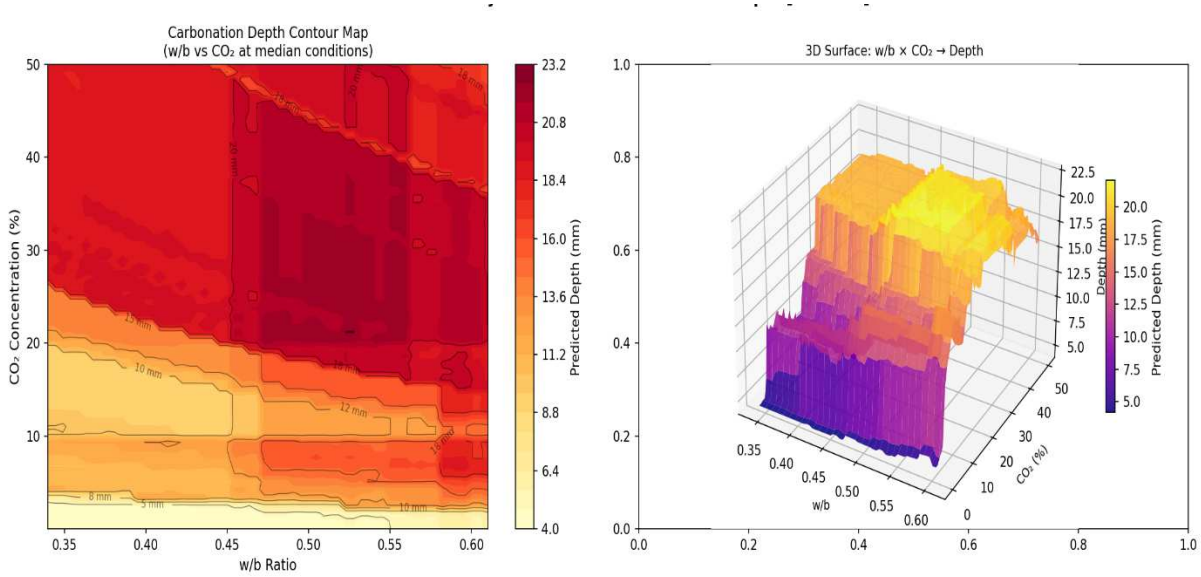


Figure 12: 2D and 3D sensitivity of carbonation depth to w/b ratio and CO_2 concentration.

Table 7: Performance of classical and ML models for carbonation depth.

Model	**R^2**	**RMSE (mm)**	**MAE (mm)**
Papadakis Model	-1.1144	18.9017	13.7294
fib Model Code 2010	-1.0161	18.4573	13.1302
DuraCrete Model	-0.9754	18.2701	12.9460
Random Forest	0.8732	4.6287	2.9362
XGBoost	0.8965	4.1815	2.5416
LightGBM	0.8936	4.2403	2.4115
Artificial Neural Network	0.7989	5.8288	4.0177

The comparison with classical carbonation models should be interpreted with caution because the compiled database contains both natural and accelerated carbonation experiments, with CO_2 concentrations ranging from atmospheric levels to highly accelerated exposure conditions. Although the classical models were implemented according to their published formulations, they were originally calibrated for more limited exposure domains and may not fully represent the wide range of carbonation conditions contained in the present database. Consequently, the reported performance differences reflect predictive capability across the entire multi-source dataset rather than a strict comparison within the calibration domain of the classical models.

The three classical carbonation models Papadakis Model, fib Model Code 2010, and DuraCrete Model produced negative R^2values and RMSE values close to 18 mm, indicating poor predictive capability on the present multi-source dataset. These models were unable to capture the combined effects of modern mix compositions and varying exposure conditions.

In contrast, the physics-guided ML models achieved much higher accuracy, with R^2values ranging from 0.80 to 0.90. Among them, XGBoost showed the best overall performance, reducing the RMSE from about 18 mm to nearly 4.2 mm and lowering the MAE from around 13 mm to 2.5 mm. These results demonstrate that physics-guided ML models can capture the complex nonlinear interactions between material properties and environmental conditions much more effectively than traditional semi-empirical carbonation equations. Specifically, XGBoost achieved approximately 77–78% lower RMSE and 80-82% lower MAE than the Papadakis, fib Model Code 2010, and DuraCrete models, demonstrating a substantial improvement in predictive reliability across the multi-source database.

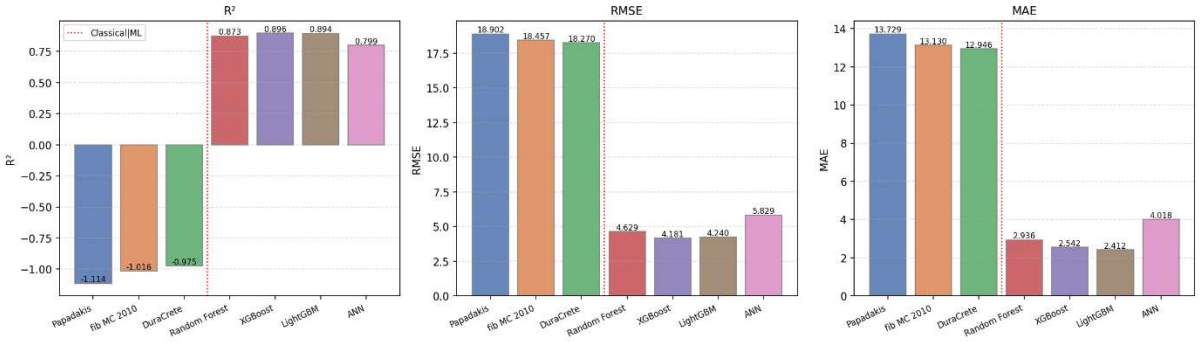


Figure 13: Classical versus ML models for carbonation depth prediction.

3.6 Uncertainty and Generalization Assessment

K-fold cross-validation was used to evaluate the robustness of the four ML models across different subsets of the 2,147-sample dataset. Table 5 shows that XGBoost and LightGBM achieved the best and most stable performance, with cross-validated R^2 values of about 0.88 and 0.86, respectively. Random Forest also showed good performance, while the Artificial Neural Network produced lower accuracy and higher variability.

Table 8: Ten-fold cross-validation performance of the machine-learning models for carbonation coefficient prediction.

Model	**CV R^2(mean ± std)**	**CV RMSE (mean ± std, mmd)**
XGBoost	0.8807 ± 0.0164	0.6719 ± 0.0451
LightGBM	0.8648 ± 0.0131	0.7166 ± 0.0396
Random Forest	0.8319 ± 0.0158	0.7998 ± 0.0528
Artificial Neural Network	0.7365 ± 0.0413	0.9996 ± 0.0915

Prediction uncertainty for the best-performing model, XGBoost, was evaluated using a bootstrap ensemble of 100 resampled models. From these ensembles, 95% prediction intervals were generated for each test sample. Figure 14 presents the uncertainty-band and parity-plot results. Most predictions follow the overall trend of the observed carbonation depths, while uncertainty gradually increases at larger depth values. The parity plot further shows that wider prediction intervals are mainly associated with high-depth samples, indicating increased uncertainty for extreme or less represented exposure conditions.

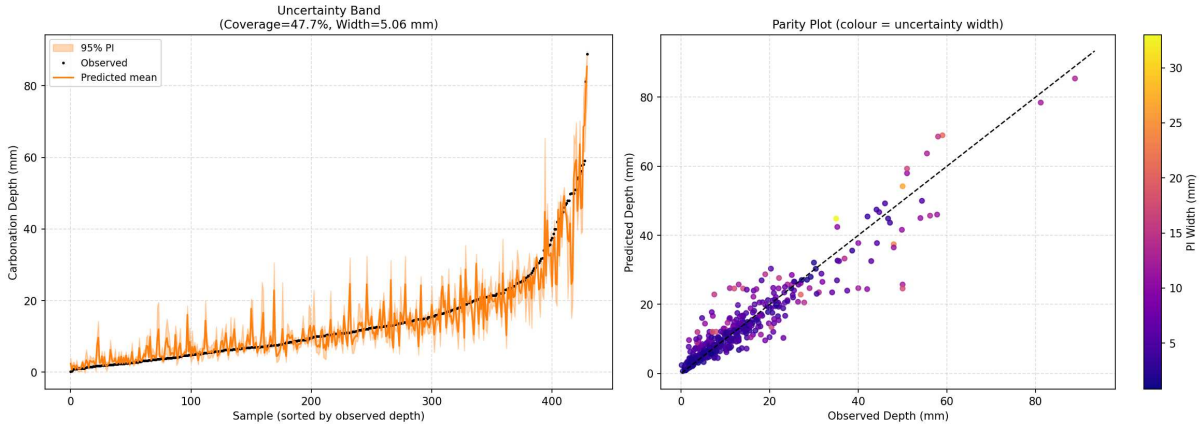


Figure 14: Prediction uncertainty and bootstrap 95% prediction intervals for the XGBoost carbonation depth model.

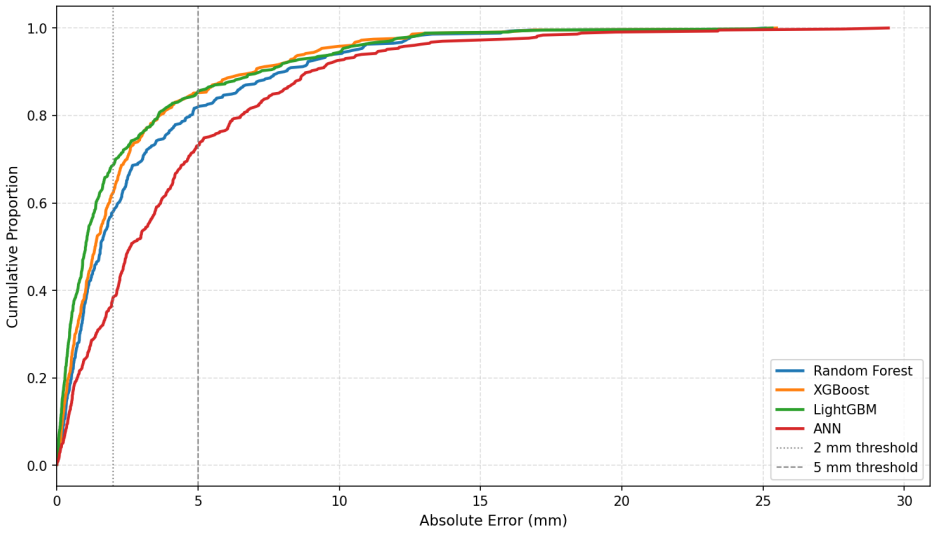


Figure 15: Cumulative Distribution of Absolute Prediction Errors

The cumulative distribution of absolute errors indicates the proportion of predictions falling within practical tolerance limits, allowing direct assessment of engineering usefulness (see in Figure 15). XGBoost and LightGBM show a faster rise in the CDF at low error levels, confirming better practical accuracy than Random Forest and ANN.

3.6.1 Group-Based Cross-Validation

Table 9: Group-based five-fold cross-validation results for carbonation coefficient prediction.

Fold	R^2	RMSE (mm/√d)	MAE (mm/√d)
Fold 1	0.8412	0.7210	0.4315
Fold 2	0.8195	0.7645	0.4520
Fold 3	0.8560	0.6912	0.4102
Fold 4	0.7845	0.8123	0.4910
Fold 5	0.8322	0.7418	0.4432
Mean	0.8267	0.7462	0.4456
Std. Dev.	±0.0271	±0.0456	±0.0298

As shown in Table 10, the proposed XGBoost model maintained stable predictive performance across all validation folds. The coefficient of determination (R^2) ranged from 0.7845 to 0.8560, while RMSE and MAE remained below 0.82 mm/√d and 0.50 mm/√d, respectively. The average cross-validation performance reached $R^2 = 0.8267 \pm 0.0271$, RMSE = 0.7462 ± 0.0456 mm/√d, and MAE = 0.4456 ± 0.0298 mm/√d. The relatively small standard deviations indicate that model performance remained consistent across different study groups. These results demonstrate that the proposed framework possesses satisfactory robustness and maintains predictive capability when evaluated under more stringent study-group-based validation conditions.

3.6.2 Error Analysis Across Carbonation Depth Ranges

To further evaluate the engineering applicability of the proposed framework, a detailed error analysis was performed across different carbonation depth ranges. The test dataset was divided into four depth intervals representing very low, low, medium, and high carbonation conditions. Prediction performance was assessed using R^2, RMSE, MAE, and MAPE to investigate how model accuracy varies with carbonation severity.

Table 10: Prediction error statistics across different carbonation depth ranges.

Depth Range	N	R^2	RMSE	MAE	MAPE
Very Low (<5 mm)	111	-2.70	2.20	1.22	57.25
Low (5–15 mm)	188	-0.63	3.57	2.10	22.95
Medium (15–30 mm)	86	-0.77	5.22	3.71	17.80
High (≥30 mm)	48	0.66	7.04	5.55	13.85

As shown in Table 10, the model maintained relatively low absolute prediction errors across all carbonation depth ranges. Although some depth intervals exhibited negative R^2 values, this behavior is largely attributed to the limited variance within individual depth groups rather than poor predictive accuracy. For example, the very-low carbonation range (<5 mm) achieved an MAE of only 1.22 mm despite a negative R^2 value. In contrast, the highest carbonation range (≥30 mm) achieved the strongest coefficient of determination (R^2 = 0.66), indicating that the model effectively captures severe carbonation behavior.

The model produced an RMSE of 4.21 mm and an MAE of 2.58 mm on the entire test dataset. 63.7% of forecasts were within ±2 mm of measured carbonation depth, with 83.1% and 94.7% falling within ±5 and ±10 mm, respectively. These results show that the suggested methodology delivers practically usable prediction accuracy for durability assessment and service-life evaluation within the analyzed parameter set.

4 Conclusion

This study established a physics-guided machine learning framework for predicting concrete carbonation by embedding the square-root-of-time carbonation law in a data-driven model, transforming carbonation depth into a carbonation coefficient and enriching the input space with physically meaningful interaction terms such as $\frac{w}{b} * CO_2$ and $RH \cdot T$. Using a comprehensive multi-source database of 2,147 samples covering wide ranges of mix proportions, curing conditions, and exposure environments, the framework produced a more compact, physically interpretable target variable and revealed structured correlations that are not apparent when depth is modeled directly. Across the four developed models, the physics-guided XGBoost algorithm achieved the highest predictive accuracy for both carbonation coefficient and reconstructed carbonation depth, with test-set coefficients of determination close to 0.89 and root mean square errors of about 0.68 mmd for the coefficient and 4.18 mm for depth, accompanied by mean absolute errors around 0.40 mmd and 2.54 mm. Ten-fold cross-validation confirmed the robustness of this performance, yielding mean cross-validated determination coefficients around 0.88 with low dispersion, while bootstrap-based prediction intervals indicated that uncertainty remains moderate for most of the test domain and increases mainly for large carbonation depths and sparsely represented conditions. Group-based five-fold cross-validation yielded an average R^2 of 0.8267 ± 0.0271, confirming that the developed framework maintains stable predictive performance across independent study groups extracted from the compiled multi-source database.

When benchmarked against established semi-empirical models (Papadakis, fib Model Code 2010, and DuraCrete), the proposed physics-guided ensemble approaches delivered a step-change in accuracy: the classical models produced negative coefficients of determination and RMSE values on the order of 18 mm with mean absolute errors around 13 mm, whereas the physics-guided XGBoost model reduced RMSE to approximately 4.2 mm and MAE to about 2.5 mm on the same dataset. These results

demonstrate that integrating physical constraints with modern ensemble learning enables the model to capture the complex, nonlinear interactions between material parameters and environmental exposure that conventional formulations fail to represent on multi-source, modern concrete data.

Explainability analyses using SHAP values, permutation importance, and interaction metrics consistently identified the interaction term $w/b \cdot CO_2$ as the dominant predictor, followed by carbonation time, the thermo-hygric interaction index $RH \cdot T$, cement content, and the standalone water-to-binder ratio, in agreement with diffusion-based carbonation theory. The two-dimensional sensitivity analysis of water-to-binder ratio and CO_2 concentration further showed that carbonation depth remains low at simultaneously low w/b and CO_2 levels but increases steeply in the high-w/b, high-CO_2 region, and that extended curing can mitigate carbonation for mixtures with higher w/b, providing directly interpretable implications for mix design and exposure control in durability-based design and service-life assessment. Taken together, the results indicate that the proposed physics-guided XGBoost model offers a reliable and physically consistent tool for predicting carbonation depth and supporting service-life-oriented design within its calibrated domain, while highlighting that predictions in sparsely sampled exposure regimes must be interpreted with caution due to the empirically quantified loss of generalization.

List of Abbreviations

RC - Reinforced concrete

CO_2 - Carbon dioxide

ML - Machine learning

PGML - Physics-guided machine learning

SCM - Supplementary cementitious material

RF - Random Forest

XGBoost - Extreme Gradient Boosting

LightGBM - Light Gradient Boosting Machine

ANN - Artificial Neural Network

MLP - Multilayer Perceptron

SHAP - SHapley Additive exPlanations

VIF - Variance Inflation Factor

RMSE - Root mean square error

MAE - Mean absolute error

R, R^2 - Correlation coefficient and coefficient of determination

CV - Cross-validation

TPE - Tree-structured Parzen Estimator

RH - Relative humidity

w/b - Water-to-binder ratio

RHT - Thermo-hygric interaction index (RH × T)

Ethics approval and consent to participate

Not applicable.

Clinical trial number

Not applicable

Consent for publication

Not applicable.

Availability of data and materials

The datasets analyzed during the current study are available from the corresponding author on reasonable request.

Competing interests

The authors declare that they have no competing interests.

Funding

The authors received no financial support for the research, authorship, or publication of this article.

Authors' contributions

Syeda Tabassum and Badhon Singha carried out the main research work, including methodology development, data analysis, and manuscript preparation. Sourav Karmakar contributed to reviewing the manuscript and providing technical suggestions. All authors approved the final version of the manuscript.

Acknowledgment

The authors express their gratitude to The Almighty and extend thanks to all those who provided support and contributed to the successful completion of this work. Their encouragement and assistance have been essential throughout the research process.

References

1. Angulo Ramirez DE, Meira GR, Quattrone M, John VM. A review on reinforcement corrosion propagation in carbonated concrete – Influence of material and environmental characteristics. Cement and Concrete Composites. 2023 Jul;140:105085. doi:10.1016/j.cemconcomp.2023.105085

2. Belda Revert A, De Weerdt K, Hornbostel K, Geiker MR. Carbonation-induced corrosion: Investigation of the corrosion onset. Construction and Building Materials. 2018 Feb;162:847–56. doi:10.1016/j.conbuildmat.2017.12.066

3. V. Robles KP, Yee JJ, Gucunski N, Kee SH. Hybrid data-driven machine learning approach for evaluating steel corrosion in concrete using electrical resistivity and documented concrete performance indicators. Construction and Building Materials. 2025 Aug;489:142154. doi:10.1016/j.conbuildmat.2025.142154

4. Azar P, Samson G, Patapy C, Cussigh F, Frouin L, Cyr M. Carbonation-induced corrosion of steel in sodium carbonate alkali-activated slag. Mater Struct. 2025 Oct;58(8):252. doi:10.1617/s11527-025-02696-9

5. Fuhaid AFA, Niaz A. Carbonation and Corrosion Problems in Reinforced Concrete Structures. Buildings. 2022 May 2;12(5):586. doi:10.3390/buildings12050586

6. Ekolu SO. Implications of global CO2 emissions on natural carbonation and service lifespan of concrete infrastructures – Reliability analysis. Cement and Concrete Composites. 2020 Nov;114:103744. doi:10.1016/j.cemconcomp.2020.103744

7. Banar R, Moodi F, Ramezanianpour AA, Ramezanianpour AM, Dashti P. Experimental and numerical simulation of carbonation-induced corrosion in reinforced concretes. Case Studies in Construction Materials. 2025 Jul;22:e04464. doi:10.1016/j.cscm.2025.e04464

8. Liu X, Niu D, Li X, Lv Y, Fu Q. Pore Solution pH for the Corrosion Initiation of Rebars Embedded in Concrete under a Long-Term Natural Carbonation Reaction. Applied Sciences. 2018 Jan 17;8(1):128. doi:10.3390/app8010128

9. Alshaeer HAY, Irwan JM, Alshalif AF, Al-Fakih A, Ewais DYZ, Salmi A, Alhokabi AA. Review on Carbonation Study of Reinforcement Concrete Incorporating with Bacteria as Self-Healing Approach. Materials. 2022 Aug 12;15(16):5543. doi:10.3390/ma15165543

10. Basdeki M, Koulouris K, Apostolopoulos C. The Influence of Corrosion of Steel Reinforcement on the Shear Strength of Existing Structure and 2nd Degree Pre-Earthquake Inspection. In: ICEAF VIII [Internet]. MDPI; 2026 [cited 2026 Mar 14]. p. 53. Available from: https://www.mdpi.com/2673-4591/119/1/53 doi:10.3390/engproc2025119053

11. Socarrás-Cordoví YC, González-Díaz L, Álvarez-Deulofeu ER. Reducciones significativas de área en aceros corroídos y su repercusión en edificaciones prefabricadas de grandes paneles. Rev Fac Ing. 2022 Jan 14;31(59):e13110. doi:10.19053/01211129.v31.n59.2022.13110

12. Kunal Tongaria KT, S.Mandal SM, Devendra Mohan DM. A Review on Carbonation of Concrete and Its Prediction Modelling. J Environ Nanotechnol. 2018;7(4):75–90. doi:10.13074/jent.2018.12.184325

13. Schultheiß AL, Patel RA, Vogel M, Dehn F. Comparative Analysis of Engineering Carbonation Model Extensions to Account for Pre-Existing Cracks. Materials. 2023 Sep 12;16(18):6177. doi:10.3390/ma16186177

14. Huo Z, Wang L, Huang Y. Predicting carbonation depth of concrete using a hybrid ensemble model. Journal of Building Engineering. 2023 Oct;76:107320. doi:10.1016/j.jobe.2023.107320

15. Rathnarajan S, Pillai RG. Carbonation models using mix-design parameters for concretes with supplementary cementitious materials. Journal of Building Engineering. 2025 Jun;104:112392. doi:10.1016/j.jobe.2025.112392

16. Cheng L, Kurihara R, Yang Z, Ohkubo T, Kitagaki R, Teramoto A, Suda Y, Maruyama I. Proposal of a new pretreatment of accelerated carbonation for evaluating material potential. Cement and Concrete Composites. 2026 Aug;171:106633. doi:10.1016/j.cemconcomp.2026.106633

17. Ekolu SO. Model for practical prediction of natural carbonation in reinforced concrete: Part 1-formulation. Cement and Concrete Composites. 2018 Feb;86:40–56. doi:10.1016/j.cemconcomp.2017.10.006